The Destabilization of Hydrogen-bonds in an External E-Field for Improved Switch Performance

Tianlv Xu[1], Roya Momen[1], Alireza Azizi[1], Tanja van Mourik[2], Herbert Früchtl[2], Steven R. Kirk[*1] and Samantha Jenkins[*1]

[1]*Key Laboratory of Chemical Biology and Traditional Chinese Medicine Research and Key Laboratory of Resource Fine-Processing and Advanced Materials of Hunan Province of MOE, College of Chemistry and Chemical Engineering, Hunan Normal University, Changsha, Hunan 410081, China*

[2]*EaStCHEM School of Chemistry, University of St Andrews, North Haugh, St Andrews, Fife KY16 9ST, Scotland, United Kingdom.*

*email: samanthajsuman@gmail.com
*email: steven.kirk@cantab.net

1. Supplementary Materials S1. A discussion of the construction of the bond-path framework set $\mathbb{B}$.

2.Supplementary Materials S2. The complete table for the real space lengths *l* and the procedure to generate the *l*.

3. Supplementary Materials S3. The mixed {***p,q}*** and {***p,p´***}path-packets.

4. Supplementary Materials S4. The {***p,q}***, {***p,p´***} and {***q,q´***} path-packets including the Fe *BCPs*.

5. Supplementary Materials S5. The stress tensor mixed {$\boldsymbol{p_\sigma,q_\sigma}$} paths-packets.

6. Supplementary Materials S6. The variation of the total local energy density $H(\mathbf{r_b})$ with the IRC.

7. Supplementary Materials S7. The variation of the stress tensor eigenvalue $\lambda_{3\sigma}$ with the IRC.

8. Supplementary Materials S8. The variation of the (*BCP-RCP*) in Å for the r, TS and the F minima.

9. Supplementary Materials S9. The variations of the ellipticity ε profiles with distance (Å) along the bond-path for N13-H14/H14--N13 *BCP*s.

10. Supplementary Materials S10. The complete table for the eigenvector following path lengths QTAIM and Stress tensor.

1. Supplementary Materials S1. A discussion of the construction of the bond-path framework set $\mathbb{B}$

The reasons for the choice of the ellipticity ε as scaling factor. This was motivated by the fact that the scaled vector tip paths drop smoothly onto the bond-path, ensuring that the tip paths are always continuous. We previously discussed the unsuitability of alternative scaling factors, $|\lambda_1 - \lambda_2|$ this was not pursued as it lacks the universal chemical interpretation of the ellipticity ε e.g. double-bond $\varepsilon > 0.25$ vs. single bond character $\varepsilon \approx 0.10$. Also unsuitable choices for scaling factors, on the basis of not attaining zero, included either ratios involving the λ_1 and λ_2 eigenvalue or any inclusion of the λ_3 eigenvalue. The λ_3 eigenvalue was also found to unsuitable because it contains no information about the least ($\underline{\mathbf{e}}_1$) and most ($\underline{\mathbf{e}}_2$) preferred directions of the total charge density $\rho(\mathbf{r})$ accumulation.

Discussion on the uniqueness of the $\mathbb{H}^*$ and $\mathbb{H}$. Because $\mathbb{H}^*$ and $\mathbb{H}$ are defined by the distances swept out by the $\underline{\mathbf{e}}_2$ tip path points $\boldsymbol{p}_i = \boldsymbol{r}_i + \varepsilon_i \underline{\mathbf{e}}_{1,i}$ and $\boldsymbol{q}_i = \boldsymbol{r}_i + \varepsilon_i \underline{\mathbf{e}}_{2,i}$ respectively and the scaling factor, ε_i is identical in equation **(3a)** and equation **(3b)** therefore for a linear bond-path $\boldsymbol{r}$ then $\mathbb{H}^* = \mathbb{H}$. The bond-path framework set $\mathbb{B} = \{\boldsymbol{p},\boldsymbol{q},\boldsymbol{r}\}$ should consider the bond-path to comprise the *unique* ***p***-, ***q***- and ***r***-paths, swept out by the $\underline{\mathbf{e}}_1$, $\underline{\mathbf{e}}_2$ and $\underline{\mathbf{e}}_3$, eigenvectors that form the eigenvector-following paths with lengths $\mathbb{H}^*$, $\mathbb{H}$ and BPL respectively. The ***p***- and ***q***-paths are unique even when the lengths of $\mathbb{H}^*$ and $\mathbb{H}$ are the same or very similar because the ***p***- and ***q***-paths traverse different regions of space. Bond-paths ***r*** with non-zero bond-path curvature which will result in $\mathbb{H}^*$ and $\mathbb{H}$ with different values, this is more likely to occur for the equilibrium geometries of closed-shell *BCP*s than for shared-shell *BCP*s. This is because the ***p***- and ***q***-paths will be different because of the greater distance travelled around the outside of a twisted bond-path ***r*** compared with the inside of the same twisted bond-path ***r***. This is because within QTAIM the $\underline{\mathbf{e}}_1$, $\underline{\mathbf{e}}_2$ and $\underline{\mathbf{e}}_3$, eigenvectors can only be defined to within to a factor of -1, i.e. ($\underline{\mathbf{e}}_1$,-$\underline{\mathbf{e}}_1$), ($\underline{\mathbf{e}}_2$,-$\underline{\mathbf{e}}_2$) and ($\underline{\mathbf{e}}_3$,-$\underline{\mathbf{e}}_3$) therefore there will be two possible tip-paths. The consequences of this (within QTAIM) calculation of the $\mathbb{H}^*$ is that we dynamically update the sign convention to define $\mathbb{H}^*$ as being the shorter of the two possible tip-paths because $\underline{\mathbf{e}}_1$ is the least preferred direction of accumulation of $\rho(\mathbf{r})$. A similar procedure is used for $\mathbb{H}$ except that we chose the longer of the two possible tip-paths because $\underline{\mathbf{e}}_2$ is the most preferred direction of accumulation of $\rho(\mathbf{r})$.

It should be noted that the direction of the ***p***- and ***q***-paths always remain orthogonal to each other since they are constructed from the $\underline{\mathbf{e}}_1$ and $\underline{\mathbf{e}}_2$ eigenvectors respectively. The ellipticity ε is used as a scaling factor in the construction of the ***p***- and ***q***-paths:

$$\boldsymbol{p}_i = \boldsymbol{r}_i + \varepsilon_i \underline{\mathbf{e}}_{1,i} \qquad \textbf{(S1a)}$$

$$\boldsymbol{q}_i = \boldsymbol{r}_i + \varepsilon_i \underline{\mathbf{e}}_{2,i} \qquad \textbf{(S1b)}$$

The lengths of the ***p***- and ***q***-paths are defined as the *eigenvector-following paths* $\mathbb{H}^*$ or $\mathbb{H}$:

$$\mathbb{H}^* = \sum^{n-1}_{i=1} |\boldsymbol{p}_{i+1} - \boldsymbol{p}_i| \qquad \textbf{(S1c)}$$

$$\mathbb{H} = \sum^{n-1}_{i=1} |\boldsymbol{q}_{i+1} - \boldsymbol{q}_i| \qquad \textbf{(S1d)}$$

Similar expressions to equations (**S1a-S1b**) and equations (**S1c-S1d**) can be constructed using the stress tensor ellipticity $\varepsilon_\sigma = |\lambda_{2\sigma}|/|\lambda_{1\sigma}| - 1$; note the different numerator and denominator orderings compared with the ellipticity ε. In the limit of vanishing ellipticity ε = 0, *for all* steps *i* along the bond-path then $\mathbb{H}$ = BPL. The form of the constituent ***p***- and ***q***-paths along each bond-path (***r***) can be used to provide a 3-D interpretation of bonding to track precisely the mechanisms of bond evolution throughout the functioning of the switch i.e. the hydrogen transfer reaction. Two paths (***q*** *and* ***q***') are associated with the $\underline{\mathbf{e}}_2$ eigenvector because $\underline{\mathbf{e}}_2 = -\underline{\mathbf{e}}_2$ lie in the same plane for the same point on the bond-path (***r***), correspondingly there are two paths (***p*** and ***p***') associated with the $\underline{\mathbf{e}}_1$ eigenvector, see **Scheme 1a**. The ***q*** (equivalently $\boldsymbol{q}_\sigma$) is always defined to be longer than the ***q'*** (equivalently $\boldsymbol{q}_\sigma$**'**) because it is constructed from the preferred direction (the $\underline{\mathbf{e}}_2$ eigenvector). Conversely, the ***p*** (equivalently $\boldsymbol{p}_\sigma$) is always defined to be the shorter of the two paths associated with the $\underline{\mathbf{e}}_1$ eigenvector. For very curved bond-paths, however, ***p*** may be shorter than ***r*** (the bond-path length), so we only chose ***p'***; see **Scheme 1a**. Therefore, we will only present the lengths of the $\mathbb{H}$ and $\mathbb{H}^{*'}$ of the {***q***,***p'***} paths and the equivalent stress tensor $\mathbb{H}_\sigma$, $\mathbb{H}_\sigma^{*'}$ of the {$\boldsymbol{q}_\sigma$,$\boldsymbol{p'}_\sigma$} paths, see **Table 3.**

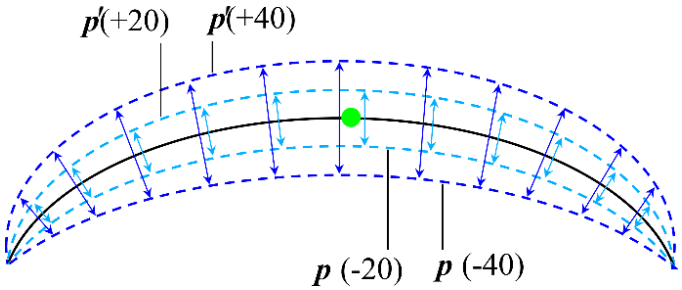

Scheme S1a. A sketch, not to scale, of the {***p***,***p'***} path-packets illustrating that for the highly curved bond-path (***r***) the ***p***-path may be shorter than ***r***-path. The example of the external electric field **E** = ±20x10^{-4} au and ±40x10^{-}4 au is provided, where the bond-path (***r***) and *BCP* are indicated by the black lines and green spheres respectively.

Implementation details of the calculation of the eigenvector-following path lengths $\mathbb{H}$ and $\mathbb{H}^*$.

When the QTAIM eigenvectors of the Hessian of the charge density $\rho(\mathbf{r})$ are evaluated at points along the bond-path, this is done by requesting them via a spawned process which runs the selected underlying QTAIM code, which then passes the results back to the analysis code. For some datasets, it occurs that, as this evaluation considers one point after another in sequence along the bond-path, the returned calculated $\underline{\mathbf{e}}_2$ (correspondingly $\underline{\mathbf{e}}_1$ is used to obtain $\mathbb{H}^*$) eigenvectors can experience a 180-degree 'flip' at the 'current' bond-path point compared with those evaluated at both the 'previous' and 'next' bond-path points in the

sequence. These 'flipped' $\underline{\mathbf{e}}_2$ (or $\underline{\mathbf{e}}_1$) eigenvectors, caused by the underlying details of the numerical implementation in the code that computed them, are perfectly valid, as these are defined to within a scale factor of -1 (i.e. inversion). The analysis code used in this work detects and re-inverts such temporary 'flips' in the $\underline{\mathbf{e}}_2$ (or $\underline{\mathbf{e}}_1$) eigenvectors to maintain consistency with the calculated $\underline{\mathbf{e}}_2$ (or $\underline{\mathbf{e}}_1$) eigenvectors at neighboring bond-path points, in the evaluation of eigenvector-following path lengths $\mathbb{H}$ and $\mathbb{H}^*$, see **Scheme S1b.**

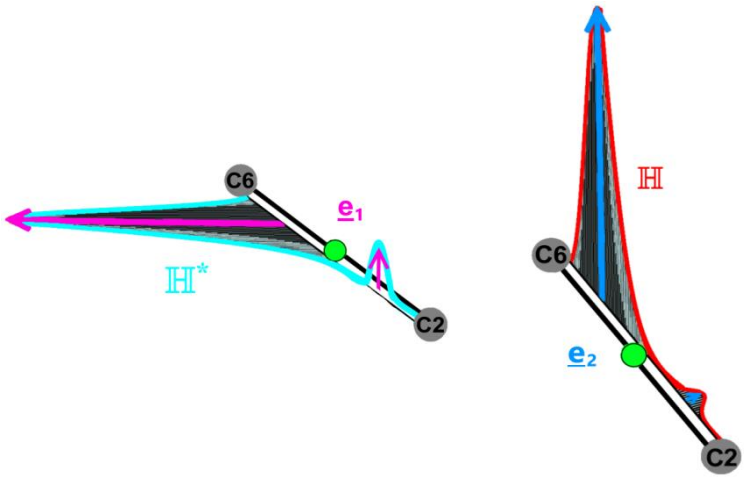

(a) **(b)**

Scheme S1b. The pale-blue line in sub-figure **(a)** represents the path, referred to as the eigenvector-following path with length $\mathbb{H}^*$, swept out by the tips of the scaled $\underline{\mathbf{e}}_1$ eigenvectors, shown in magenta, and defined by equation **(1c)**. The red path in sub-figure **(b)** corresponds to $\mathbb{H}$, constructed from the path swept out by the tips of the scaled $\underline{\mathbf{e}}_2$ eigenvectors, shown in mid-blue and is defined by equation **(1d)**. The pale-blue and mid-blue arrows representing the $\underline{\mathbf{e}}_1$ and $\underline{\mathbf{e}}_2$ eigenvectors are scaled by the ellipticity ε respectively, where the vertical scales are exaggerated for visualization purposes. The green sphere indicates the position of a given *BCP*.

2. Supplementary Materials S2.

Table S2. The real space lengths *l* in atomic units (a.u.) for the reverse (r ='ON') and forward (f = 'OFF') directions of the (±40, 0, ±20), see the caption of **Table 3** for further details.

			l		
	-40	**+40**	**00**	**-20**	**+20**
BCP	(*r*,*f*)	(*r*,*f*)	(*r*,*f*)	(*r*,*f*)	(*r*,*f*)
C1-C2	(0.220, 0.112)	(0.239, 0.143)	(0.227, 0.125)	(0.222, 0.117)	(0.233, 0.134)
C1-C4	(0.314, 0.199)	(0.337, 0.249)	(0.322, 0.226)	(0.317, 0.213)	(0.329, 0.238)
C3-C4	(0.232, 0.200)	(0.223, 0.224)	(0.223, 0.211)	(0.226, 0.205)	(0.222, 0.217)
C2-C5	(0.332, 0.222)	(0.318, 0.242)	(0.321, 0.233)	(0.325, 0.228)	(0.319, 0.237)
C3-C6	(0.245, 0.214)	(0.228, 0.246)	(0.232, 0.231)	(0.237, 0.222)	(0.229, 0.238)
C5-C6	(0.320, 0.156)	(0.319, 0.175)	(0.318, 0.163)	(0.318, 0.160)	(0.318, 0.168)
C4-H7	(0.506, 0.376)	(0.518, 0.437)	(0.505, 0.408)	(0.503, 0.393)	(0.510, 0.423)
C1-H8	(0.443, 0.281)	(0.506, 0.357)	(0.473, 0.320)	(0.456, 0.301)	(0.490, 0.339)
C5-H9	(0.599, 0.381)	(0.588, 0.426)	(0.590, 0.406)	(0.593, 0.394)	(0.589, 0.416)
C10-C2	(0.272, 0.232)	(0.280, 0.254)	(0.272, 0.242)	(0.270, 0.237)	(0.275, 0.248)
C10-H11	(0.378, 0.266)	(0.374, 0.349)	(0.377, 0.290)	(0.376, 0.268)	(0.376, 0.319)
C10-H12	(0.337, 0.364)	(0.364, 0.421)	(0.344, 0.394)	(0.338, 0.380)	(0.352, 0.407)
C3-N13	(0.257, 0.187)	(0.233, 0.194)	(0.241, 0.176)	(0.249, 0.177)	(0.236, 0.182)
H15-N13	(0.668, 0.640)	(0.560, 0.684)	(0.610, 0.704)	(0.637, 0.681)	(0.584, 0.704)
H14-N13	(0.784, 0.783)	(0.591, 0.955)	(0.654, 0.891)	(0.701, 0.836)	(0.617, 0.930)
C6-N16	(0.226, 0.309)	(0.225, 0.327)	(0.224, 0.315)	(0.224, 0.311)	(0.224, 0.320)
H14-N16	(1.129, 0.485)	(1.006, 0.577)	(1.054, 0.533)	(1.087, 0.510)	(1.025, 0.554)
H17-N16	(0.724, 0.775)	(0.631, 0.873)	(0.661, 0.811)	(0.689, 0.791)	(0.639, 0.838)
C1-Fe18	(0.197, 0.329)	(0.208, 0.292)	(0.197, 0.301)	(0.195, 0.311)	(0.202, 0.295)
C4-Fe18	(0.243, 0.266)	(0.251, 0.270)	(0.243, 0.271)	(0.242, 0.270)	(0.246, 0.271)
C5-Fe18	(0.253, 0.139)	(0.240, 0.176)	(0.244, 0.155)	(0.247, 0.147)	(0.241, 0.164)
H14 (GC)	(1.484, 1.028)	(1.296, 1.252)	(1.375, 1.178)	(1.425, 1.109)	(1.330, 1.225)

Procedure to generate the real-space trajectory lengths *l*.

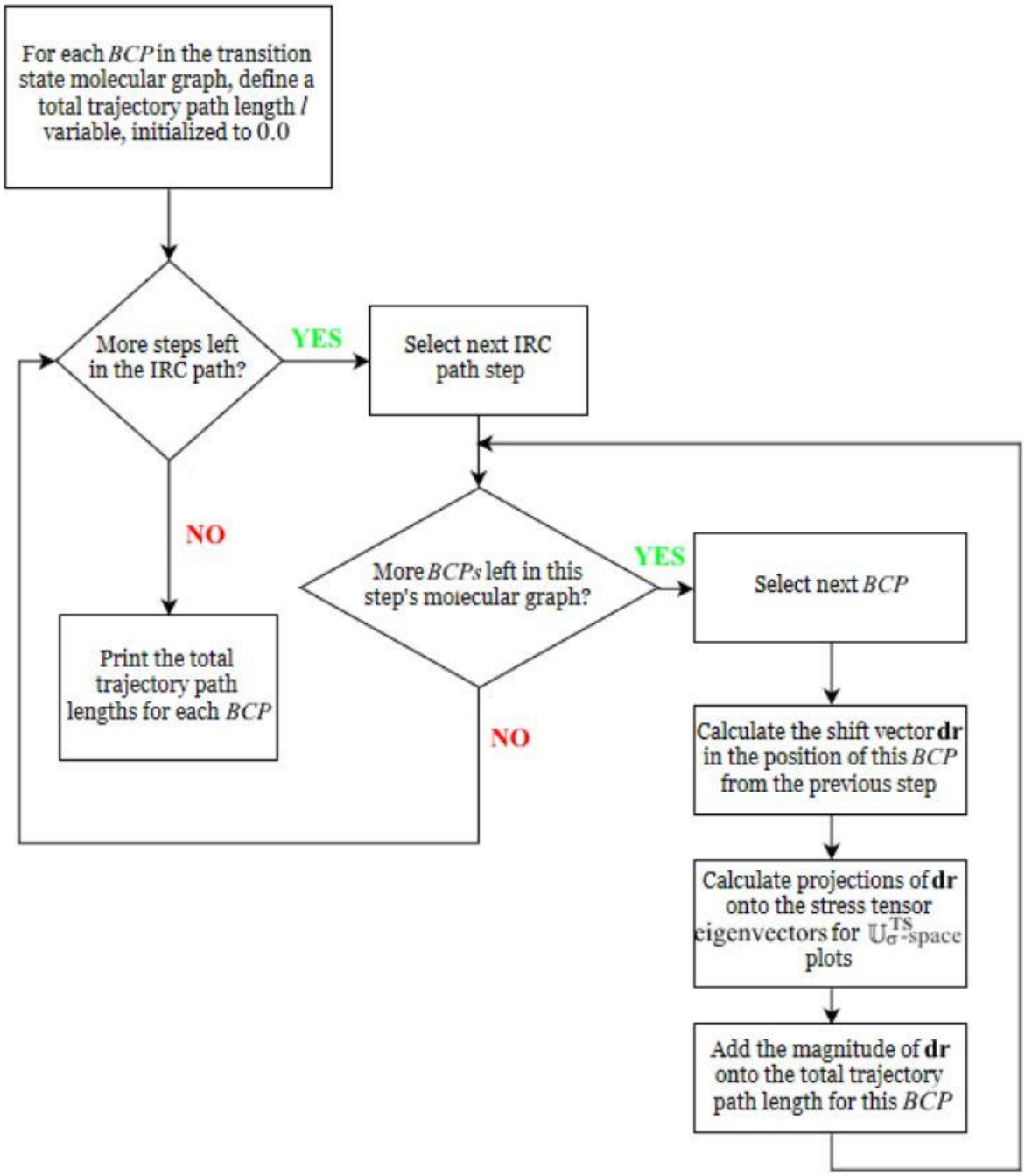

Note: for displaying the stress tensor trajectories $\mathbb{T}_\sigma^{TS}(s)$, large steps that can occur at the beginning or end of a trajectory $\mathbb{T}_\sigma^{TS}(s)$ may swamp the appearance of the trajectory $\mathbb{T}_\sigma^{TS}(s)$. To solve this we temporarily filter these steps before including them back in to correctly calculate the real space $\mathbb{T}_\sigma^{TS}(s)$ length *l*.

3. Supplementary Materials S3.

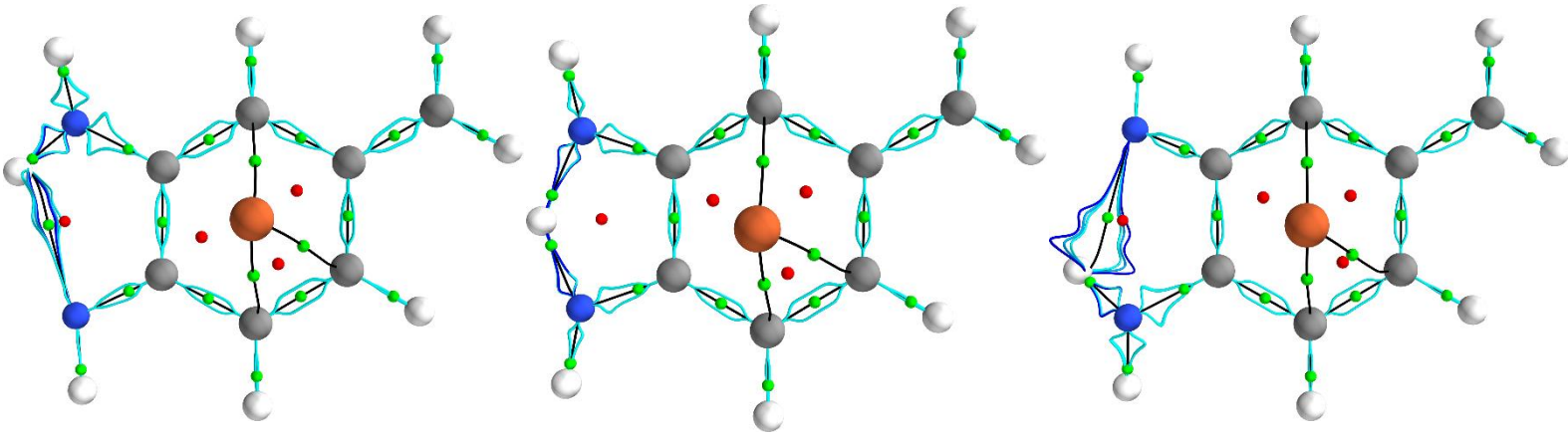

(a)

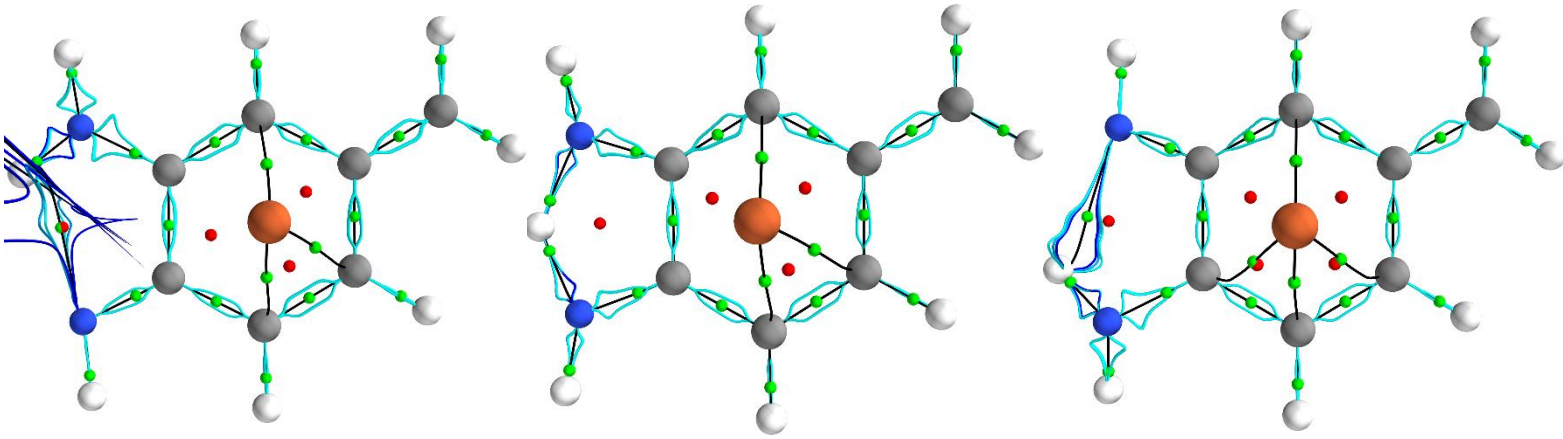

(b)

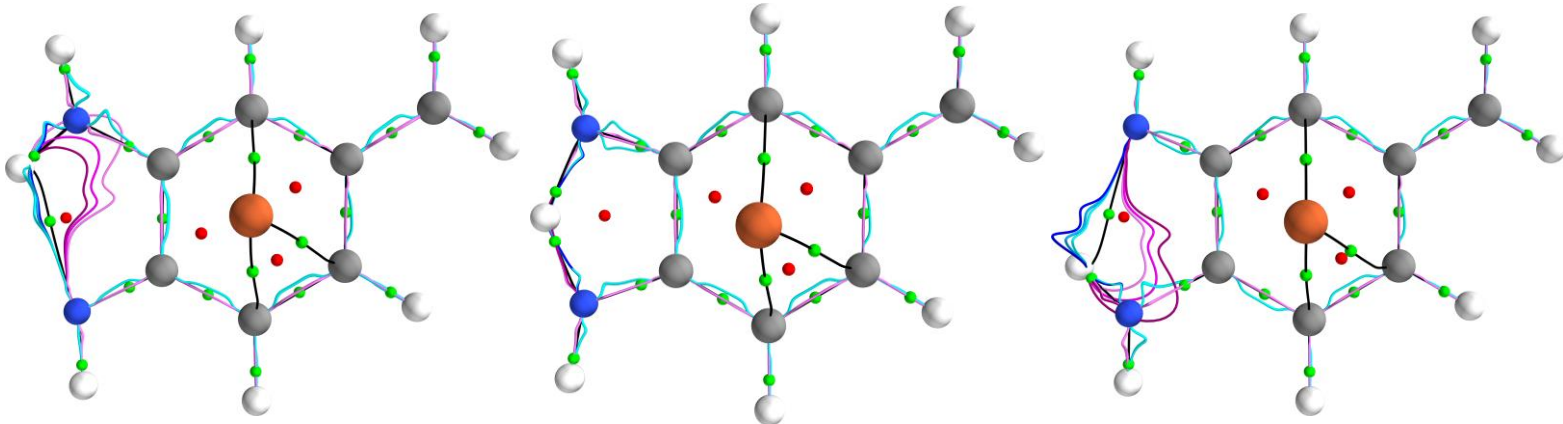

(c)

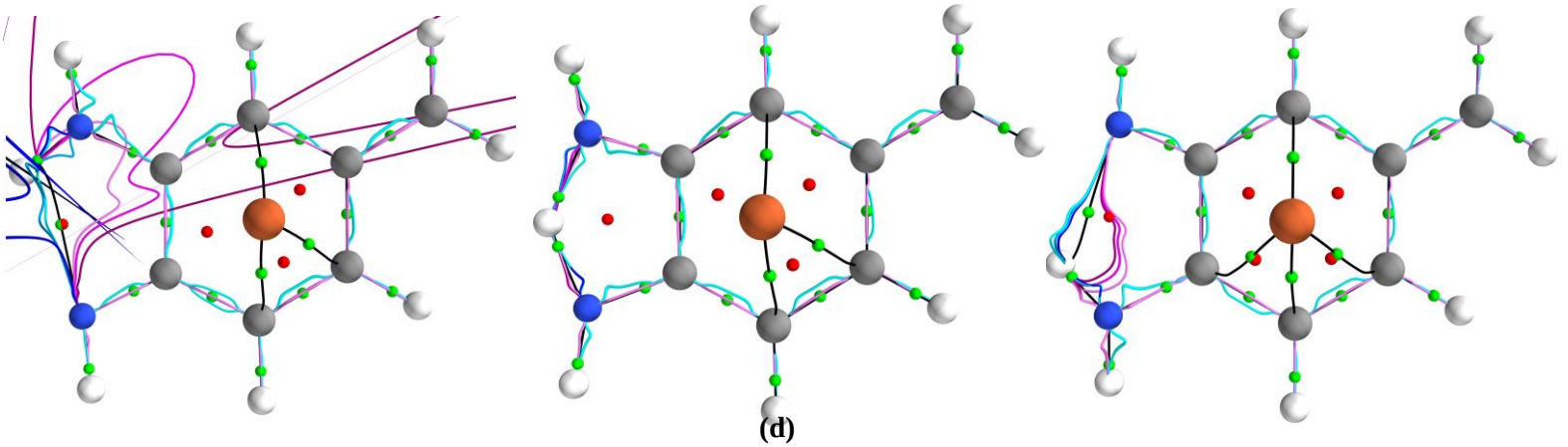

(d)

Figure S3. The {***p,p'***} paths-packets (blue) for the external field; **E** = 0, $20x10^{-4}$au and $40x10^{-4}$au, for the reverse (r) , transition state (TS) and forward (f) directions are indicated by dark-blue, pale-blue, are presented in (a) and (b) respectively. The corresponding {***p***,***q***} path-packets for values of the applied field; $-40x10^{-4}$au, 0, $-20x10^{-4}$au are presented in sub-figure **(b)**. See the caption of **Figure 3** for further details.

4. Supplementary Materials S4.

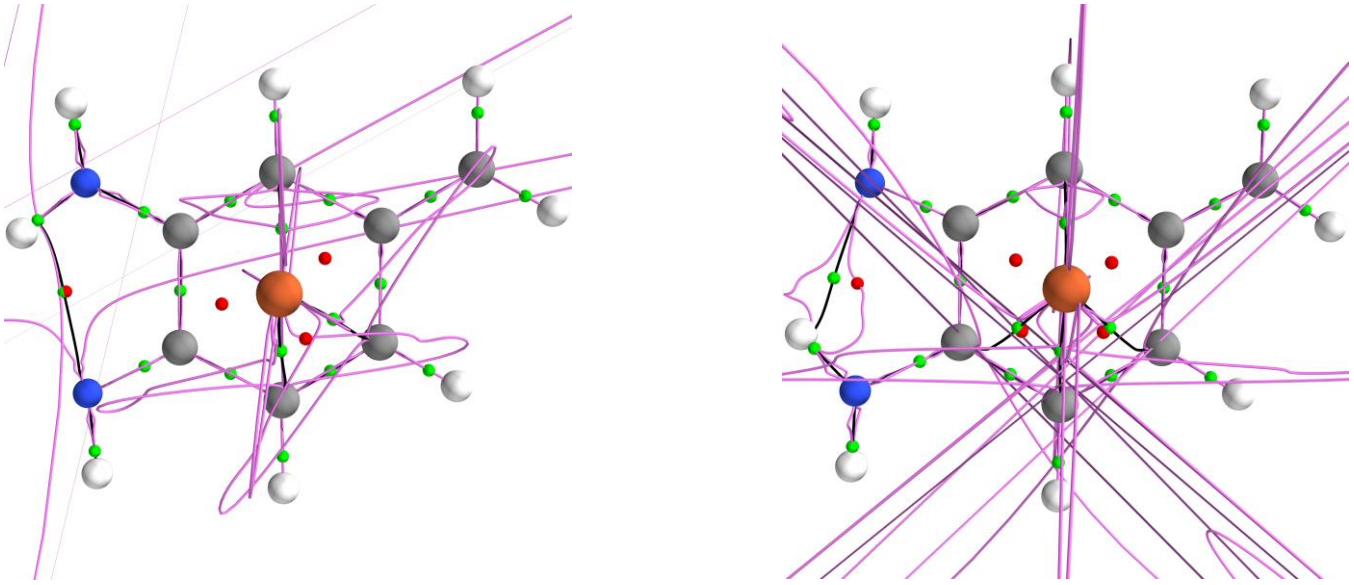

(a)

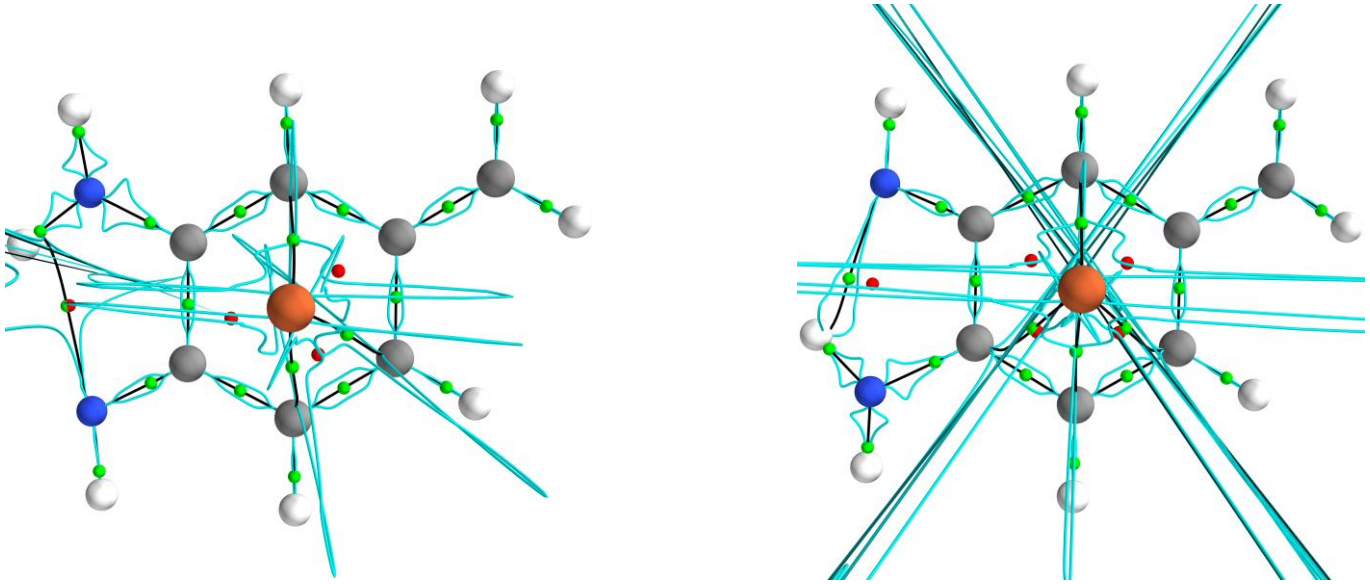

(b)

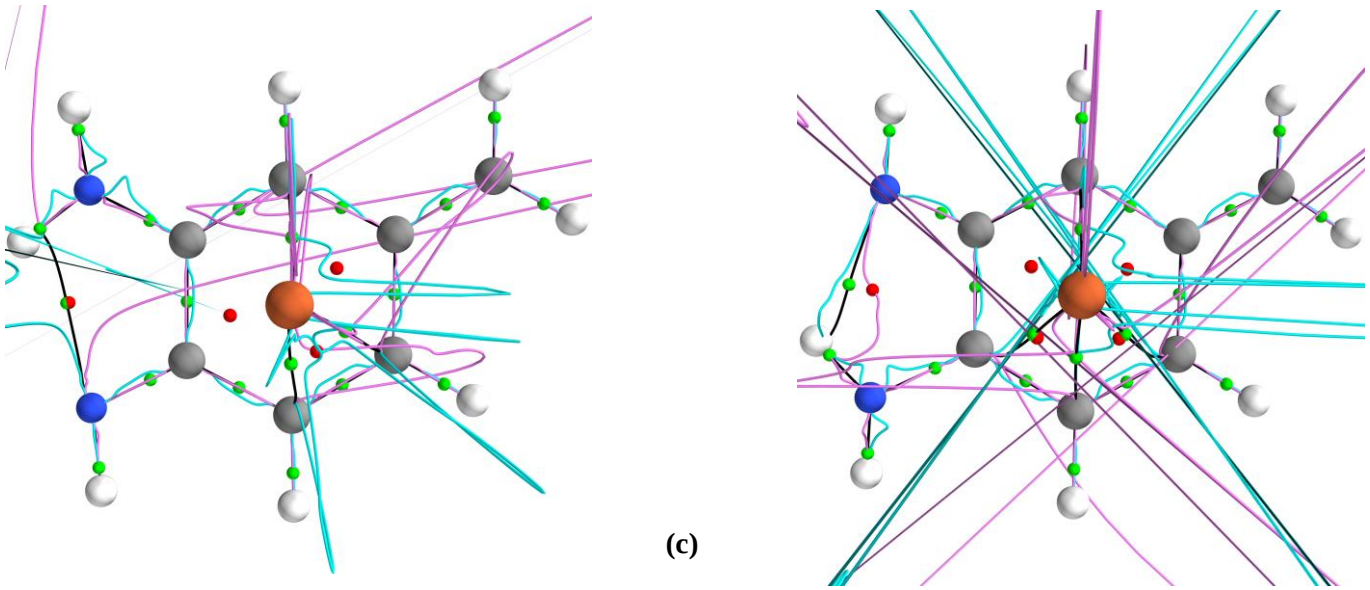

(c)

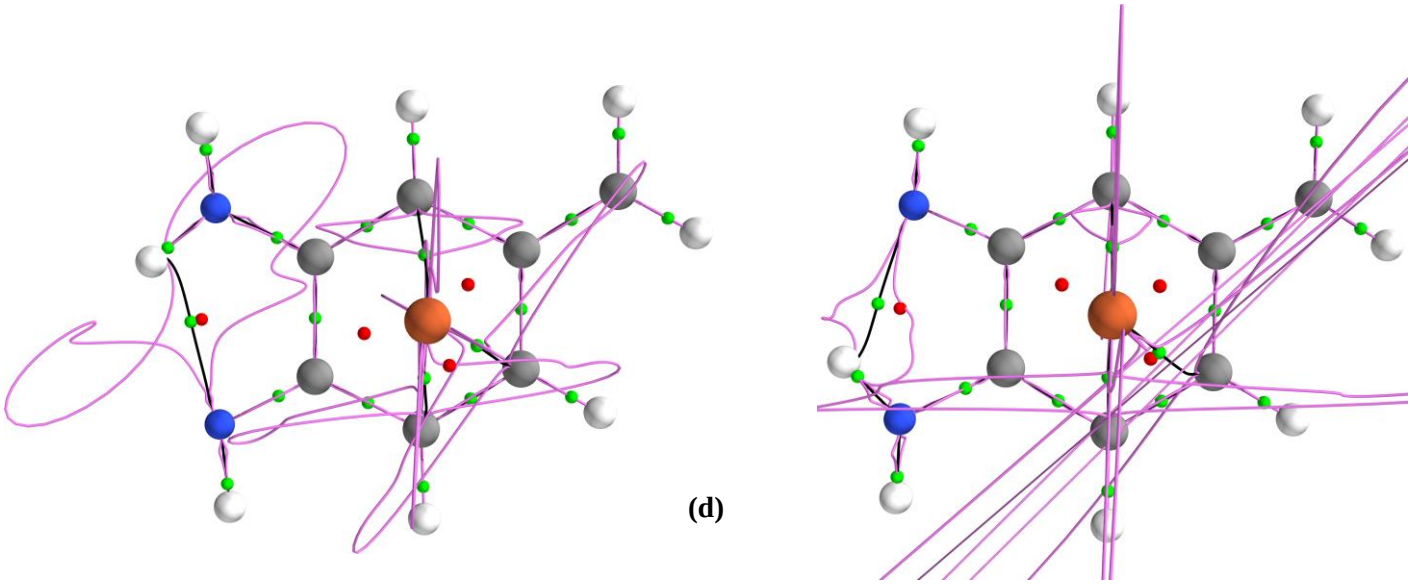

(d)

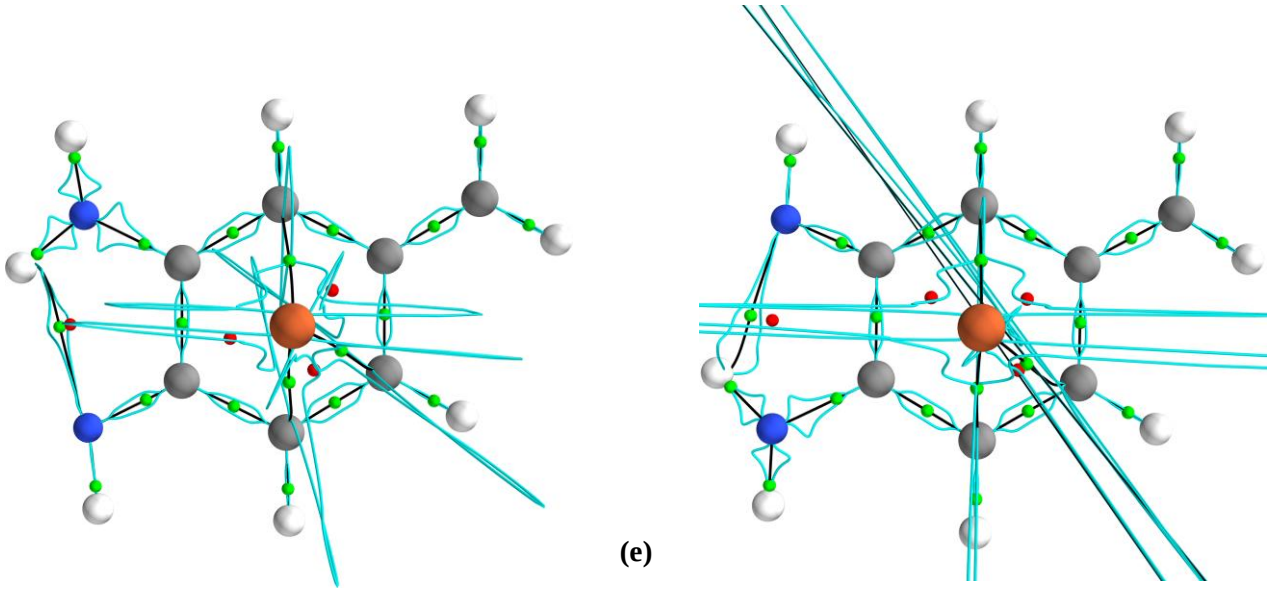

(e)

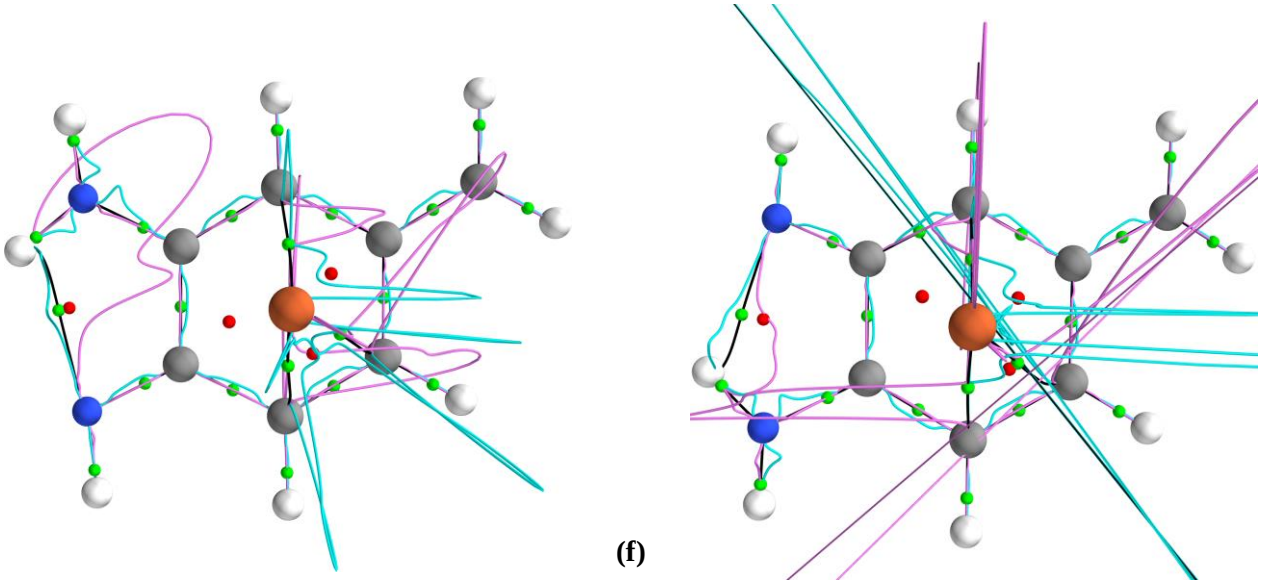

(f)

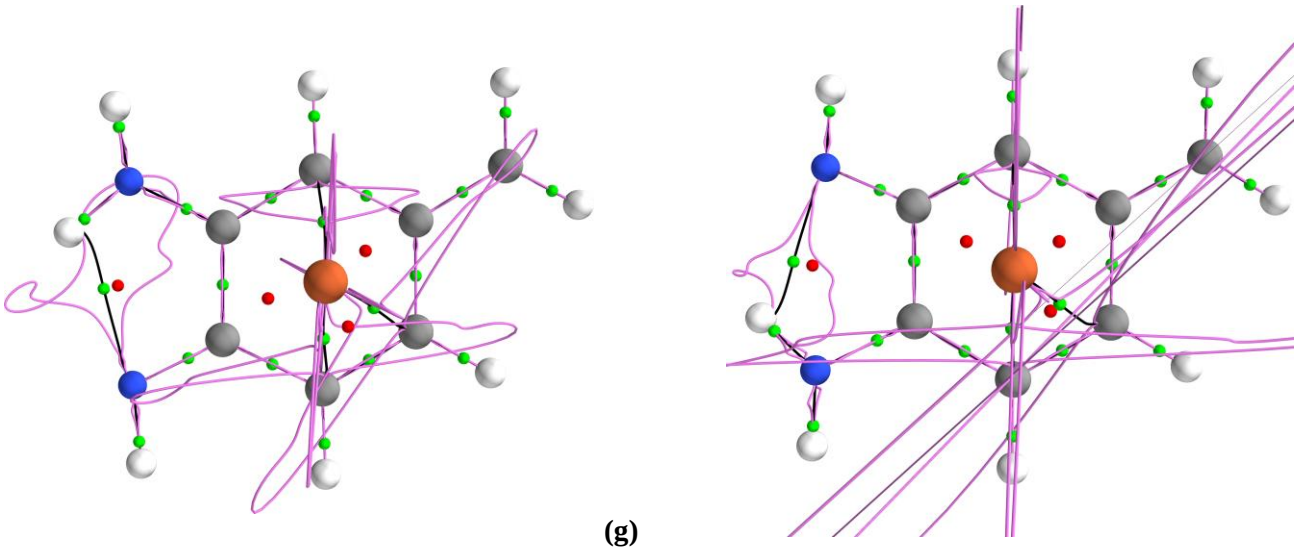

(g)

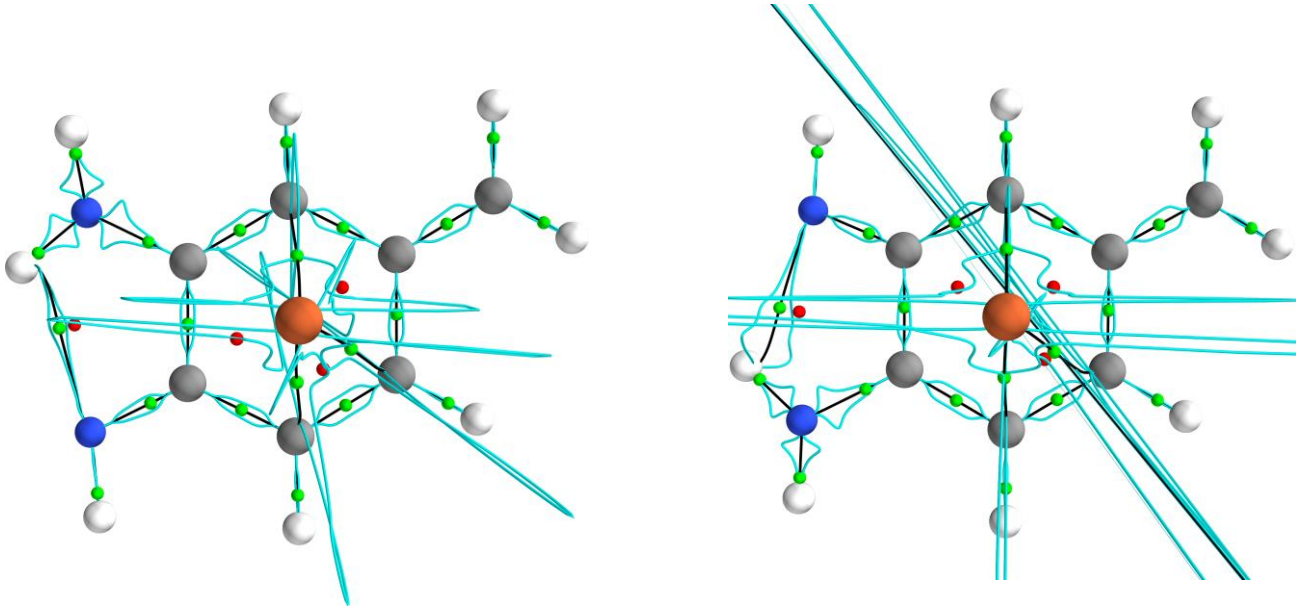

(h)

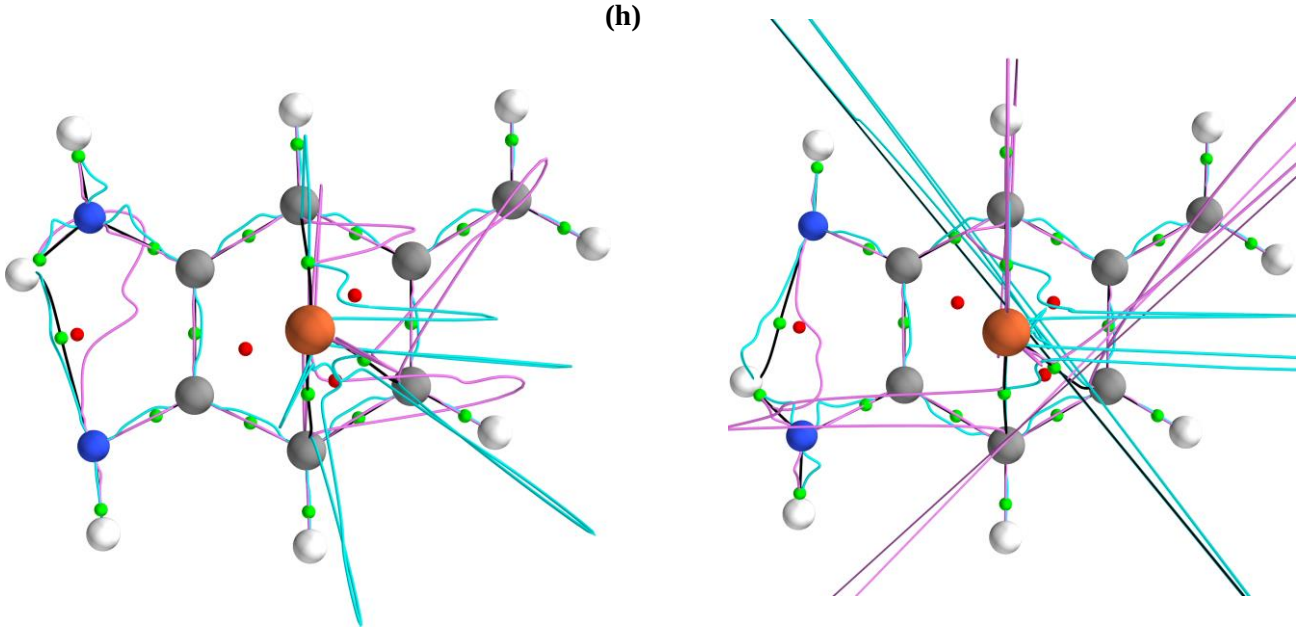

(i)

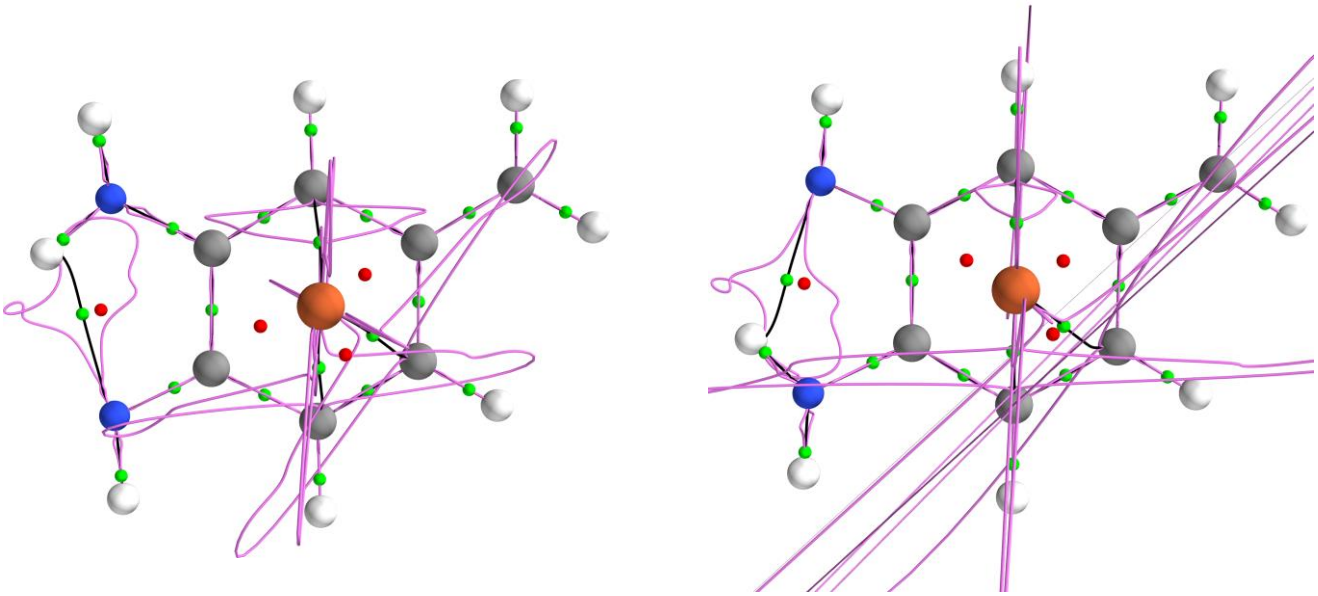

(j)

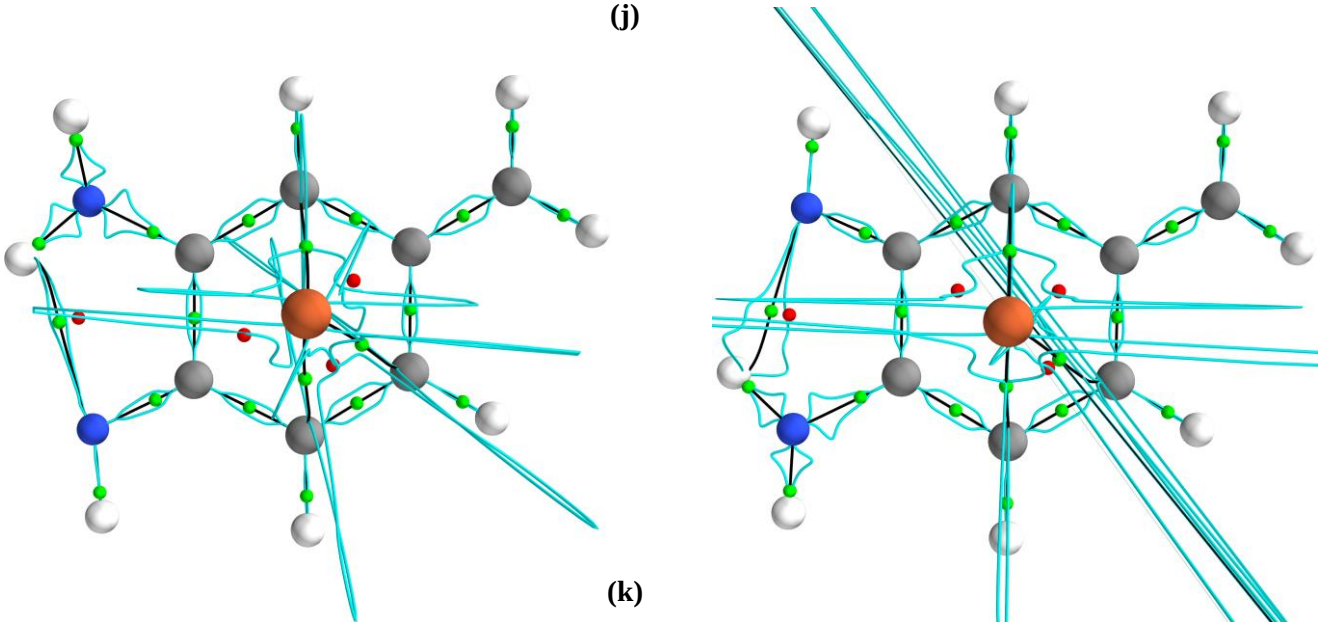

(k)

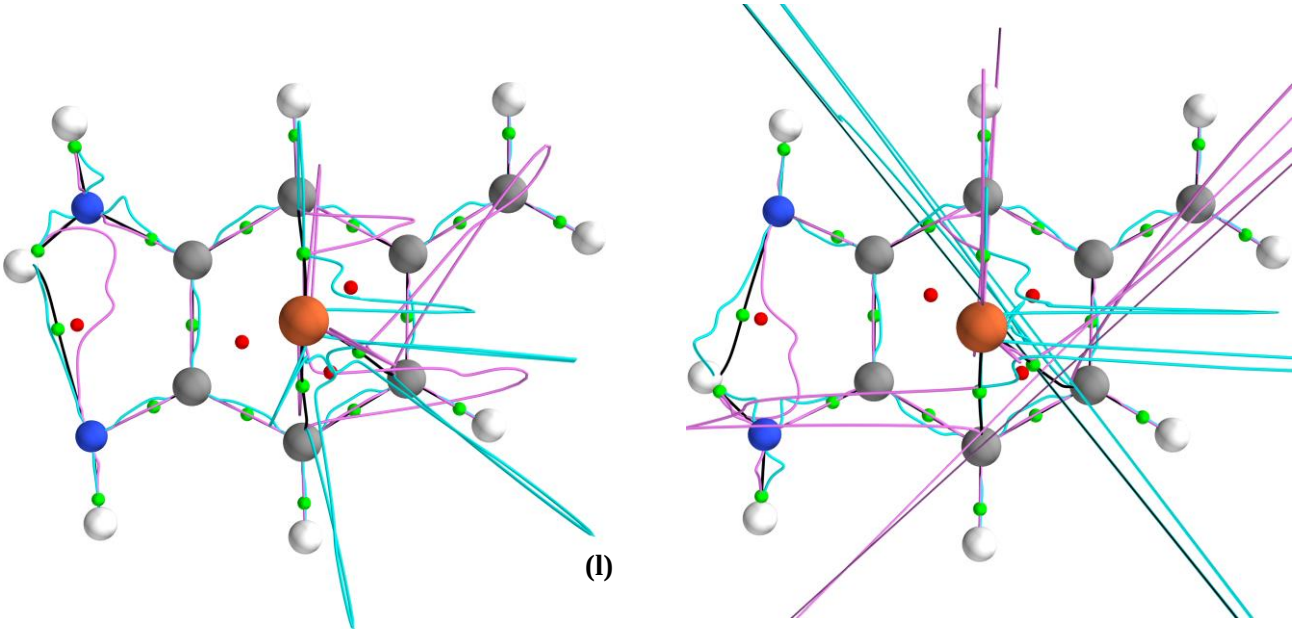

(l)

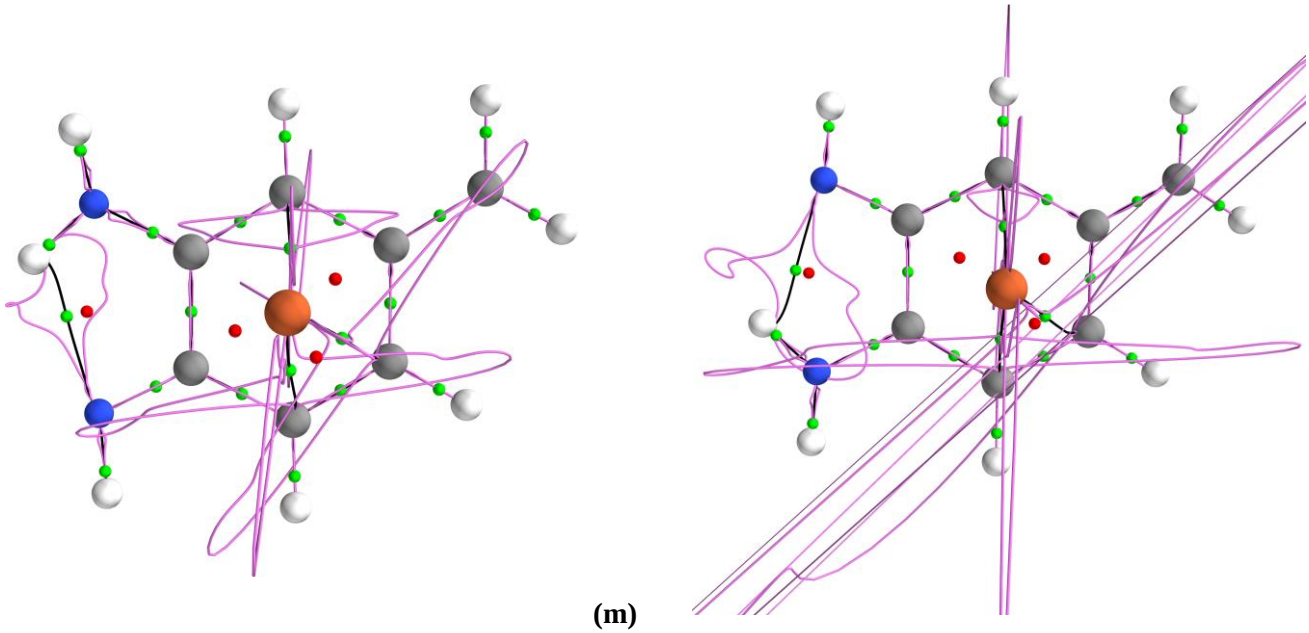

(m)

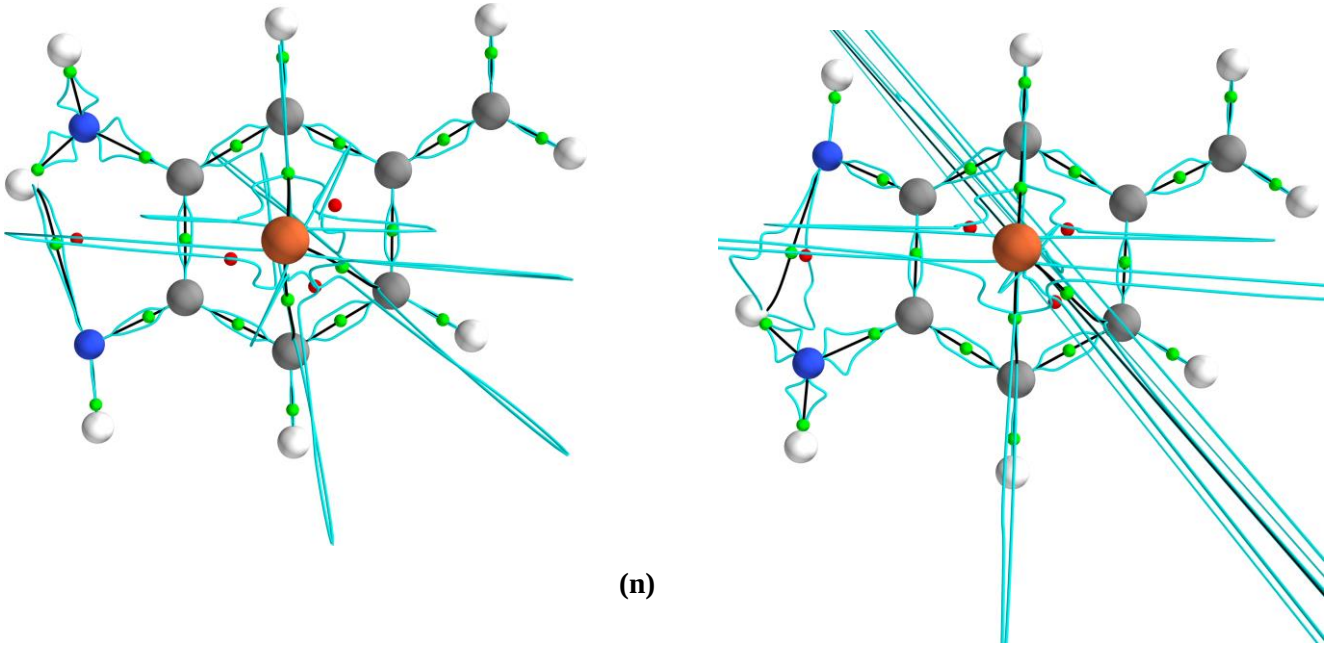

(n)

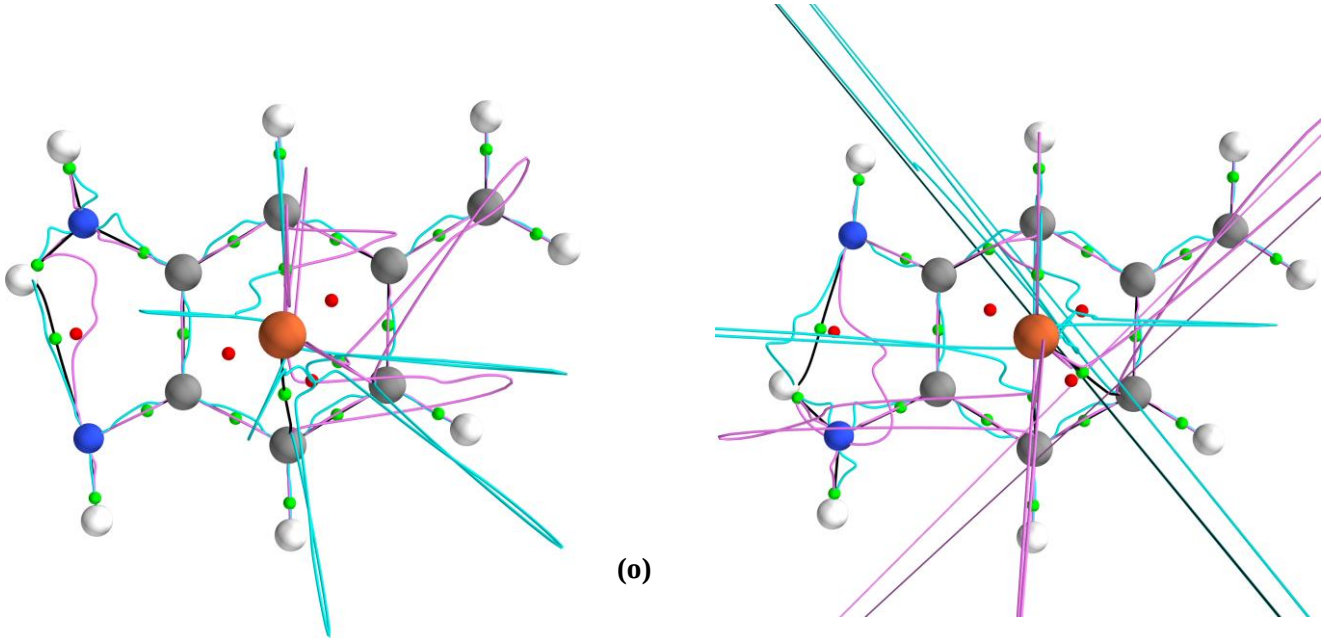

(o)

Figure S4. Sub-figures **(a-c)** correspond to the ***q,q´*** (pale-magenta) path-packets, ***p- p´*** (pale-blue) path-packets and the ***p*** (pale-blue), ***q*** (pale-magenta) path-packets for the values of the applied field -40x10^{-4}au for the reverse (r) and forward (f) directions in the left and right panels respectively. The corresponding {***q,q}***, {***p,p´***} and {***p,q***} for the values of the applied field -20x10^{-4}au are presented in sub-figures **(d-f)** respectively. The corresponding {***q,q´***}, {***p,p´***} and {***p,q***} for the values of the applied field 0 are presented in sub-figures **(g-i)** respectively. The corresponding {***q,q´***}, {***p,p´***}paths and {***p,q***} for the values of the applied field 20x10^{-4}au are presented in sub-figures **(j-l)** respectively. The corresponding {***q,q´***}**,** {***p,p´***} and {***p,q***} for the values of the applied field 40x10^{-4}au are presented in sub-figures **(m-o)** respectively. See the caption of **Figure 3** for further details.

5. Supplementary Materials S5.

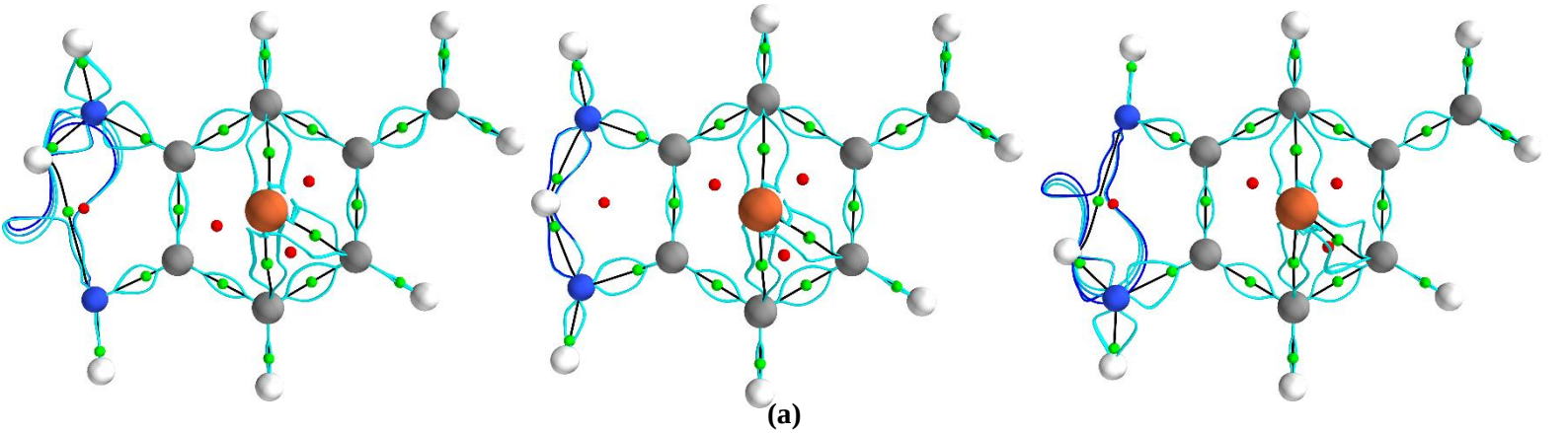

(a)

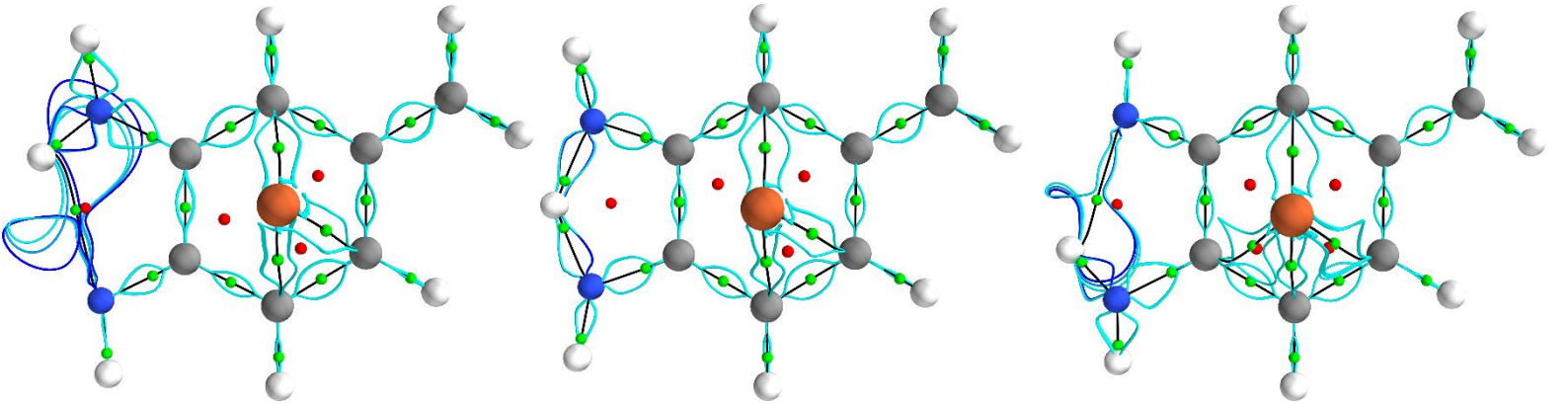

(b)

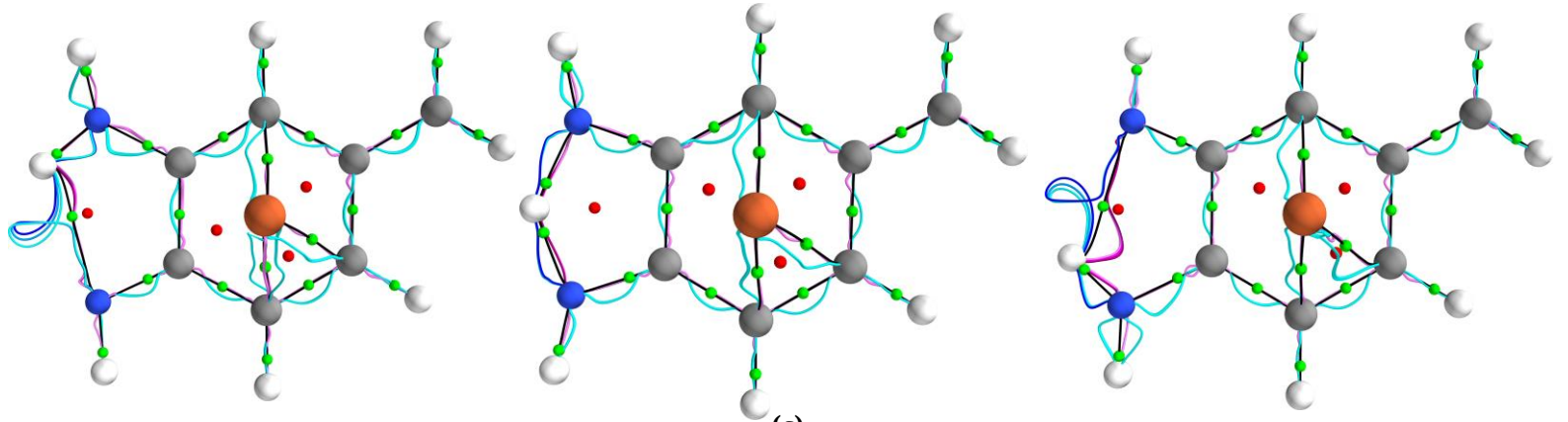

(c)

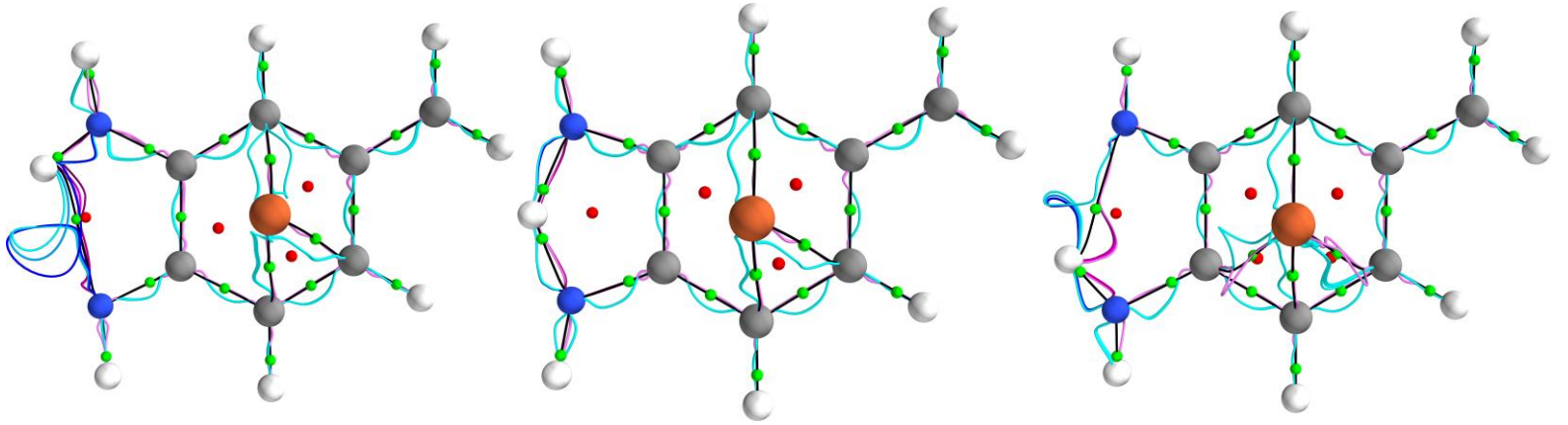

(d)

Figure S5. The $\boldsymbol{p_\sigma}$ (blue) $\boldsymbol{q_\sigma}$ (magenta) for the values of the applied field; $40\text{x}10^{-4}$au, 0, $20\text{x}10^{-4}$au for the reverse (r),transition state(TS) and forward (f) directions are presented in the left ,middle and right panels respectively in sub-figure **(a)**. The corresponding {$\boldsymbol{p_\sigma}$,$\boldsymbol{q_\sigma}$ for values of the applied field; $-40\text{x}10^{-4}$au, 0, $-20\text{x}10^{-4}$au are presented in sub-figure **(b)**. See the caption of **Figure 5** for further details.

6. Supplementary Materials S6.

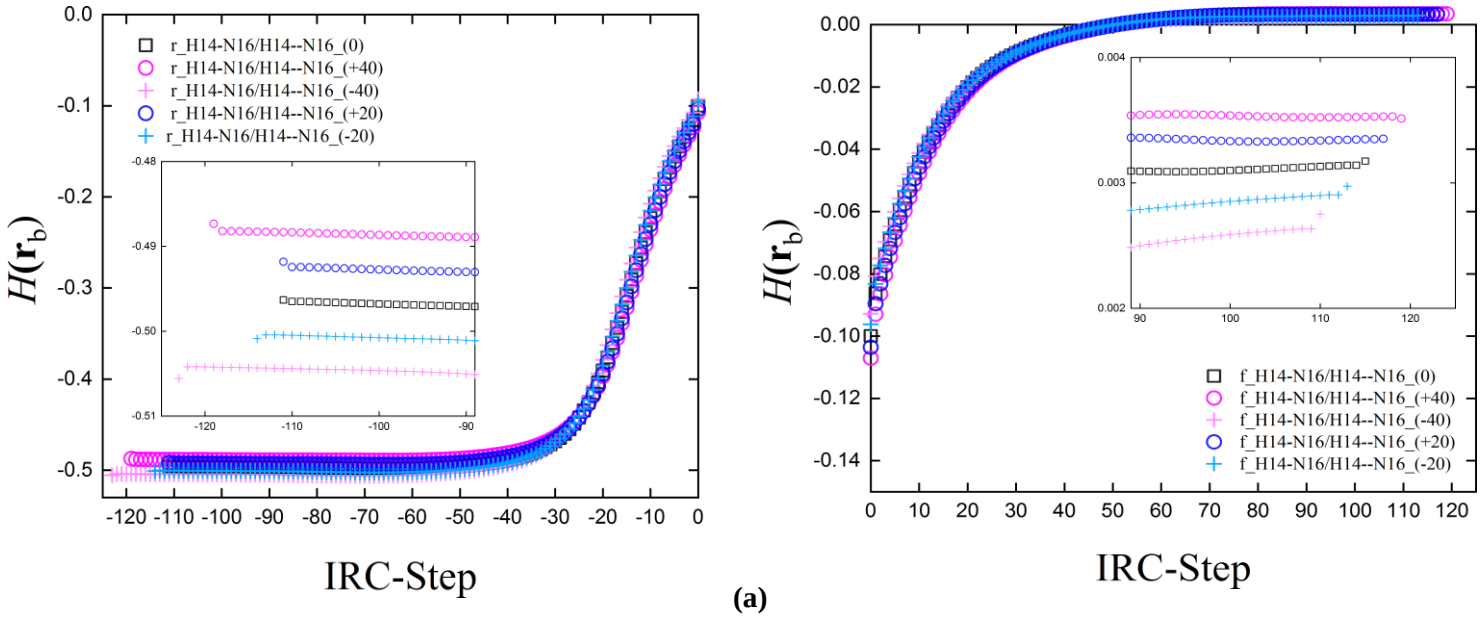

(a)

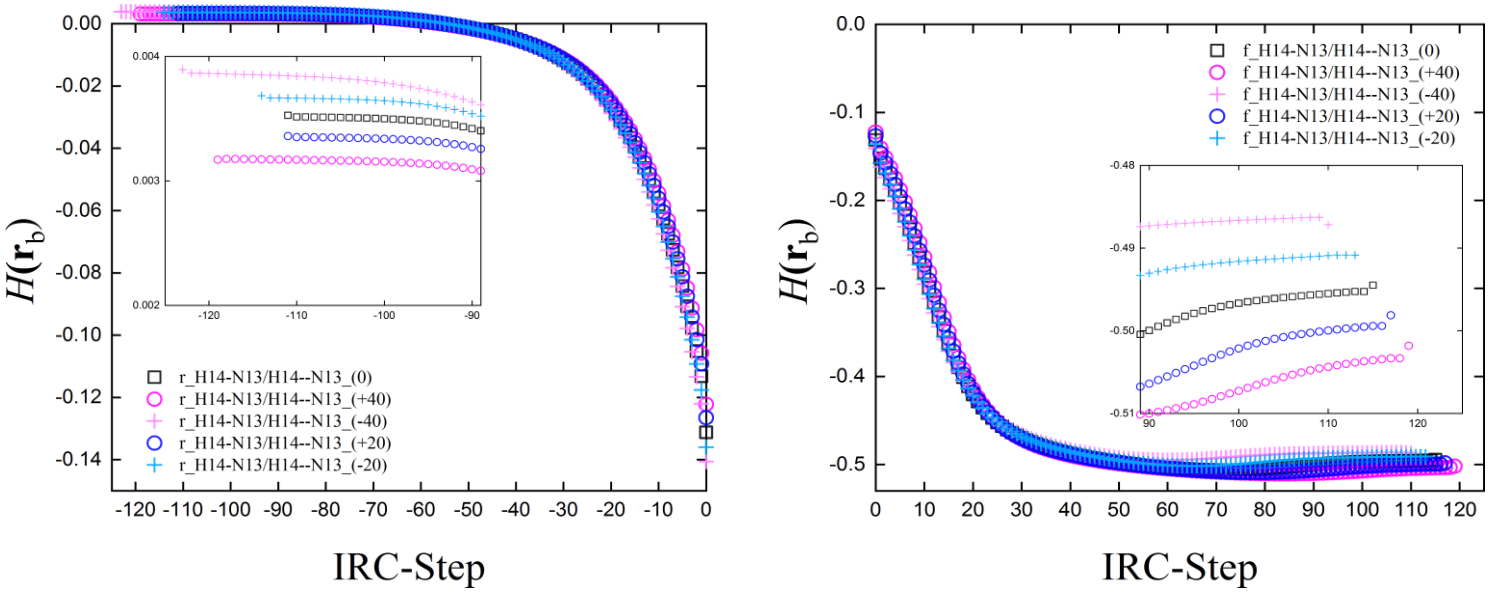

(b)

Figure S6. The variation of the total local energy density $H(\mathbf{r_b})$ with the IRC step of the H14-N16/H14--N16 *BCP*s for the reverse (r) and forward (f) directions for values of the applied electric field $\pm 40 \times 10^{-4}$au, 0, $\pm 20 \times 10^{-4}$au are presented in the left and right panels respectively in sub-figure **(a)**. The corresponding plots for the H14-N13/H14--N13 *BCP*s in sub-figure **(b)**, see **Scheme 1** for the *BCP* locations and the atom labels.

7. Supplementary Materials S7.

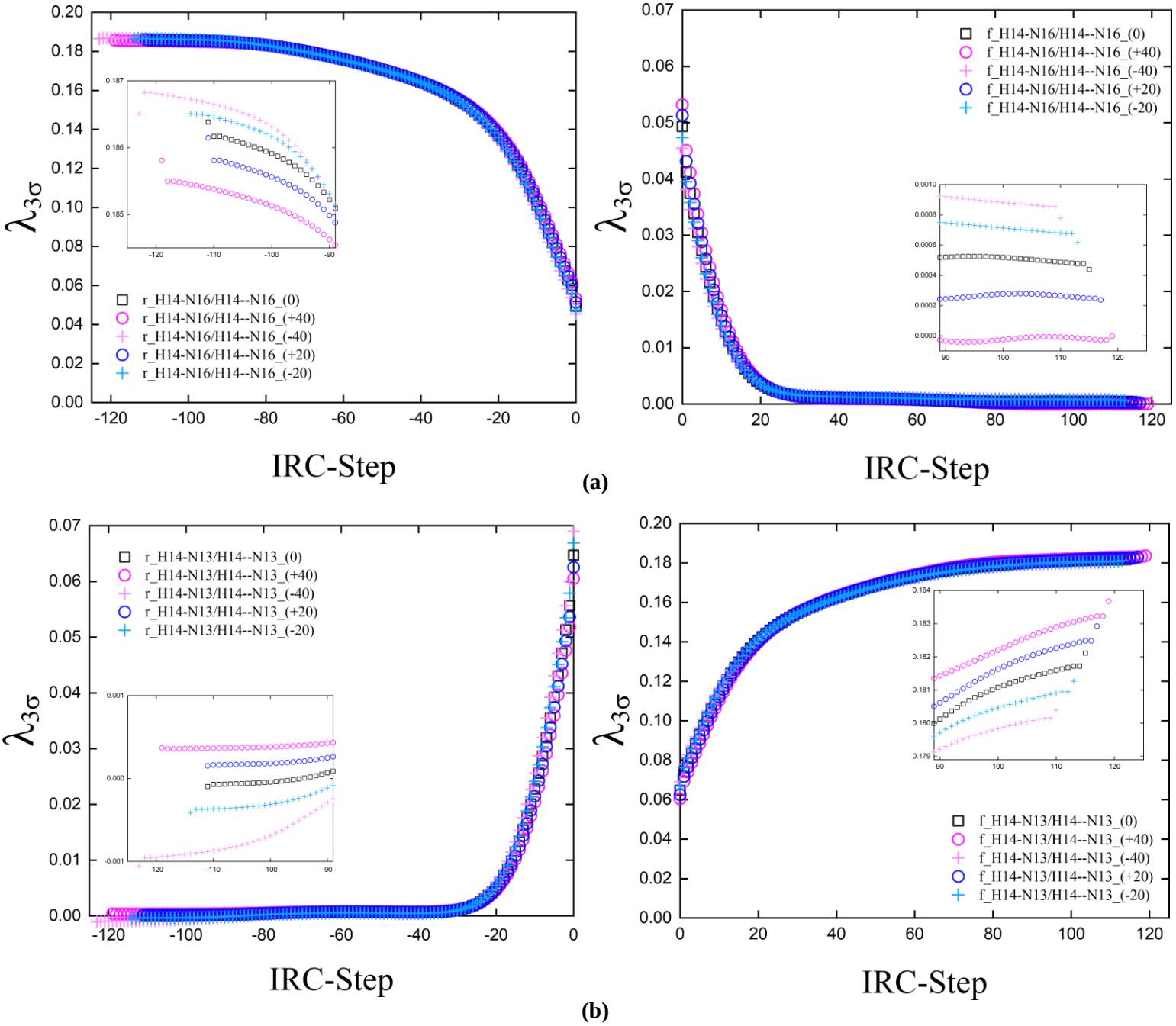

Figure S7. The variation of the stress tensor eigenvalue $\lambda_{3\sigma}$ with the IRC of the H14-N16/H14--N16 *BCP*s and H14-N13/H14--N13 *BCP*s for values of the applied electric field ±40x10^{-4}au, 0, ±20x10^{-4}au are presented in the left and right panels of sub-figures **(a)** and **(b)** respectively. See **Scheme 1** for the *BCP* locations and the atom labels.

8. Supplementary Materials S8.

Table S8. The variation of the (*BCP-RCP*) in Å corresponding to the reverse (*r*), transition state(TS) and forward (*f*) directions of the (±40,0,±20), See the caption of **Table 1** for further details.

	0		
H14-N16	{(0.965,0.760,0.260)}		
H14-N13	{(0.188,0.779,0.956)}		
Fe18-C1	{(0.393,0.390,0.138)}		
Fe18-C4	{(0.339,0.309,0.506)}		

	-20	**+20**
H14-N16	{(0.967,0.757,0.287)}	{(0.963,0.763,0.228)}
H14-N13	{(0.135,0.781,0.953)}	{(0.229,0.776,0.959)}
Fe18-C1	{(0.398,0.388,0.117)}	{(0.388,0.391,0.154)}
Fe18-C4	{(0.333,0.310,0.520)}	{(0.344,0.309,0.496)}

	-40	**+40**
H14-N16	{(0.959,0.755,0.311)}	{(0.961,0.765,0.188)}
H14-N13	{(0.029,0.784,0.950)}	{(0.263,0.773,0.962)}
Fe18-C1	{(0.402,0.384,0.086)}	{(0.383,0.390,0.166)}
Fe18-C4	{(0.328,0.313,0.539)}	{(0.349,0.312,0.487)}
Fe18-C4	{(0.051)}	

9. Supplementary Materials S9.

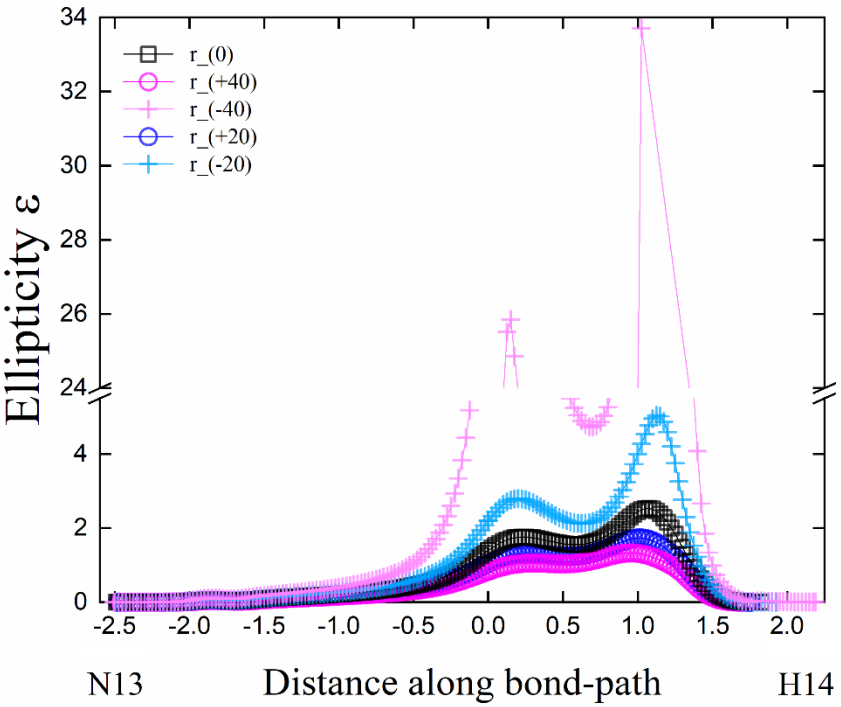

Figure S9. The variations of the ellipticity ε profiles with distance (Å) along the bond-path for the reverse (r) and forward (f) directions for the values of the applied field; $40x10^{-4}$au, 0, $20x10^{-4}$au for the associated with the H14-N13/H14--N13. For further details, see **Figure 5**.

Table S10(a). The bond path lengths BPL and the inter-nuclear *NCP-NCP* separations GBL in atomic units (a.u.) for the reverse (*r*), transition state (TS) and forward (*f*) directions of the (±40,0, ±20), see the caption of **Table 4** for further details.

		BPL		GBL	
BCP	**E-field**	(*r*,TS,*f*)	(*r*,TS,*f*)	(*r*,TS,*f*)	(*r*,TS,*f*)
	{**-40**}{**+40**}	{(1.905, 1.877, 1.877),(1.902, 1.879, 1.872)}		{(1.940, 1.916, 1.916),(1.939, 1.919, 1.912)}	
H15-N13	{**0**}	{(1.903, 1.878, 1.874)}		{(1.940, 1.917, 1.914)}	
	{**-20**}{**+20**}	{(1.904, 1.878, 1.875),(1.903, 1.879, 1.873)}		{(1.940, 1.917, 1.915),(1.939, 1.918, 1.913)}	
	{**-40**}{**+40**}	{(4.695, 2.381, 1.904),(4.165, 2.436, 1.891)}		{(4.131, 2.385, 1.944),(3.992, 2.437, 1.931)}	
H14-N13	{**0**}	{(4.317, 2.407, 1.897)}		{(4.061, 2.410, 1.938)}	
	{**-20**}{**+20**}	{(4.427, 2.393, 1.901),(4.234, 2.422, 1.893)}		{(4.096, 2.397, 1.941),(4.027, 2.424, 1.935)}	
	{**-40**}{**+40**}	{(1.885, 2.551, 4.069),(1.897, 2.491, 4.319)}		{(1.926, 2.544, 3.923),(1.938, 2.487, 4.060)}	
H14-N16	{**0**}	{(1.891, 2.519, 4.175)}		{(1.932, 2.514, 3.989)}	
	{**-20**}{**+20**}	{(1.888, 2.535, 4.118),(1.894, 2.503, 4.241)}		{(1.929, 2.529, 3.955),(1.935, 2.500, 4.024)}	
	{**-40**}{**+40**}	{(1.872, 1.881, 1.901),(1.879, 1.881, 1.904)}		{(1.912, 1.920, 1.937),(1.917, 1.919, 1.940)}	
H17-N16	{**0**}	{(1.875, 1.881, 1.902)}		{(1.915, 1.919, 1.938)}	
	{**-20**}{**+20**}	{(1.874, 1.881, 1.901),(1.877, 1.881, 1.903)}		{(1.913, 1.920, 1.938),(1.916, 1.919, 1.939)}	

Table S10(b). The eigenvector following path lengths for the QTAIM and Stress tensor of the most and least preferred for the reverse (*r*),transition state(TS) and forward (*f*) directions of the (±40,0,±20), see the caption of **Table 4** for further details.

			{$\mathbb{H}^*$,$\mathbb{H}^*$'}		
BCP		(*r*,TS,*f*)	(*r*,TS,*f*)	(*r*,TS,*f*)	(*r*,TS,*f*)
	{**-40**}{**+40**}	{(1.955, 1.972, 2.266),(1.890, 1.972, 1.991)}		{(1.929, 1.943, 2.299),(1.889, 1.943, 1.959)}	
H15-N13	{**0**}	{(1.940, 1.957, 2.295),(1.889, 1.957, 1.975)}			
	{**-20**}{**+20**}	{(1.947, 1.964, 2.284),(1.890, 1.964, 1.983)}		{(1.934, 1.950, 2.299),(1.889, 1.950, 1.966)}	
	{**-40**}{**+40**}	{(11405, 2.531, 2.491),(2.573, 2.531, 2.198)}		{(6.262, 2.551, 2.510),(2.597, 2.551, 2.233)}	
H14-N13	{**0**}	{(9.015, 2.543, 2.501),(2.588, 2.543, 2.225)}			
	{**-20**}{**+20**}	{(15.183, 2.536, 2.494),(2.580, 2.536, 2.213)}		{(7.124, 2.550, 2.507),(2.596, 2.550, 2.237)}	
	{**-40**}{**+40**}	{(2.614, 2.663, 5.571),(2.244, 2.663, 2.722)}		{(2.591, 2.648, 10.899),(2.221, 2.648, 2.694)}	
H14-N16	{**0**}	{(2.602, 2.661, 6.598),(2.246, 2.661, 2.711)}			
	{**-20**}{**+20**}	{(2.608, 2.657, 5.943),(2.253, 2.657, 2.718)}		{(2.596, 2.654, 8.024),(2.235, 2.654, 2.702)}	
	{**-40**}{**+40**}	{(2.303, 1.936, 1.925),(1.951, 1.936, 1.891)}		{(2.262, 1.980, 1.963),(1.998, 1.980, 1.898)}	
H17-N16	{**0**}	{(2.275, 1.957, 1.942),(1.974, 1.957, 1.894)}			
	{**-20**}{**+20**}	{(2.288, 1.946, 1.933),(1.962, 1.946, 1.892)}		{(2.267, 1.969, 1.952),(1.986, 1.969, 1.896)}	

{ℍ,ℍ'}

BCP		(*r*,TS,*f*)	(*r*,TS,*f*)	(*r*,TS,*f*)	(*r*,TS,*f*)
	{**-40**}{**+40**}	{(1.890, 1.969, 1.989),(1.953, 1.969, 2.268)}	{(1.889, 1.942, 1.957),(1.928, 1.942, 2.302)}		
H15-N13	{**0**}	{(1.889, 1.955, 1.973),(1.939, 1.955, 2.297)}			
	{**-20**}{**+20**}	{(1.890, 1.962, 1.981),(1.946, 1.962, 2.286)}	{(1.889, 1.948, 1.965),(1.933, 1.948, 2.302)}		
	{**-40**}{**+40**}	{(2.543, 2.501, 2.462),(11404, 2.501, 2.192)}	{(2.576, 2.530, 2.218),(5.620, 2.530, 2.488)}		
H14-N13	{**0**}	{(2.560, 2.514, 2.219),(8.013, 2.514, 2.472)}			
	{**-20**}{**+20**}	{(2.551, 2.507, 2.207),(13.712, 2.507, 2.466)}	{(2.568, 2.522, 2.225),(6.344, 2.522, 2.479)}		
	{**-40**}{**+40**}	{(2.233, 2.691, 2.694),(2.595, 2.691, 5.001)}	{(2.225, 2.615, 2.661),(2.624, 2.615, 9.661)}		
H14-N16	{**0**}	{(2.248, 2.629, 2.680),(2.634, 2.629, 5.847)}			
	{**-20**}{**+20**}	{(2.242, 2.687, 2.688),(2.589, 2.687, 5.294)}	{(2.239, 2.622, 2.671),(2.629, 2.622, 7.077)}		
	{**-40**}{**+40**}	{(1.949, 1.935, 1.891),(2.308, 1.935, 1.924)}	{(1.996, 1.979, 1.898),(2.267, 1.979, 1.963)}		
H17-N16	{**0**}	{(1.973, 1.956, 1.894),(2.281, 1.956, 1.941)}			
	{**-20**}{**+20**}	{(1.961, 1.945, 1.892),(2.294, 1.945, 1.932)}	{(1.985, 1.968, 1.895),(2.272, 1.968, 1.952)}		

{$\mathbb{H}_\sigma^*$,$\mathbb{H}_\sigma^*$'}

BCP		(*r*,TS,*f*)	(*r*,TS,*f*)	(*r*,TS,*f*)	(*r*,TS,*f*)
	{**-40**}{**+40**}	{(1.883, 1.883, 1.882),(1.907, 1.883, 1.897)}	{(1.884, 1.883, 1.882),(1.904, 1.883, 1.896)}		
H15-N13	{**0**}	{(1.883, 1.883, 1.882),(1.905, 1.883, 1.894)}			
	{**-20**}{**+20**}	{(1.883, 1.882, 1.881),(1.906, 1.882, 1.895)}	{(1.883, 1.883, 1.882),(1.905, 1.883, 1.895)}		
	{**-40**}{**+40**}	{(2.457, 2.400, 1.928),(5.052, 2.400, 2.348)}	{(2.518, 2.456, 1.916),(4.208, 2.456, 2.401)}		
H14-N13	{**0**}	{(2.489, 2.427, 1.922),(4.396, 2.427, 2.371)}			
	{**-20**}{**+20**}	{(2.472, 2.413, 1.925),(4.555, 2.413, 2.358)}	{(2.504, 2.442, 1.919),(4.289, 2.442, 2.385)}		
	{**-40**}{**+40**}	{(1.911, 2.578, 2.632),(2.518, 2.578, 4.092)}	{(1.920, 2.519, 2.576),(2.458, 2.519, 4.440)}		
H14-N16	{**0**}	{(1.915, 2.549, 2.608),(2.485, 2.549, 4.217)}			
	{**-20**}{**+20**}	{(1.913, 2.563, 2.621),(2.502, 2.563, 4.150)}	{(1.917, 2.534, 2.593),(2.470, 2.534, 4.309)}		
	{**-40**}{**+40**}	{(1.884, 1.885, 1.885),(1.896, 1.885, 1.902)}	{(1.886, 1.887, 1.887),(1.901, 1.887, 1.905)}		
H17-N16	{**0**}	{(1.885, 1.885, 1.885),(1.898, 1.885, 1.903)}			
	{**-20**}{**+20**}	{(1.884, 1.885, 1.885),(1.897, 1.885, 1.903)}	{(1.885, 1.886, 1.886),(1.899, 1.886, 1.904)}		

{$\mathbb{H}_\sigma$,$\mathbb{H}_\sigma$'}

BCP		(*r*,TS, *f*)	(*r*,TS, *f*)	(*r*,TS, *f*)	(*r*,TS,*f*)
	{**-40**}{**+40**}	{(1.907, 1.883, 1.896),(1.883, 1.883, 1.882)}	{(1.904, 1.883, 1.895),(1.884, 1.883, 1.883)}		
H15-N13	{**0**}	{(1.905, 1.883, 1.895),(1.883, 1.883, 1.882)}			
	{**-20**}{**+20**}	{(1.906, 1.883, 1.896),(1.883, 1.883, 1.882)}	{(1.905, 1.883, 1.895),(1.883, 1.883, 1.882)}		
	{**-40**}{**+40**}	{(4.949, 2.390, 2.338),(2.443, 2.390, 1.926)}	{(4.314, 2.444, 2.391),(2.500, 2.444, 1.914)}		
H14-N13	{**0**}	{(4.500, 2.416, 2.361),(2.473, 2.416, 1.919)}			
	{**-20**}{**+20**}	{(4.639, 2.402, 2.348),(2.457, 2.402, 1.923)}	{(4.396, 2.430, 2.376),(2.487, 2.430, 1.916)}		
	{**-40**}{**+40**}	{(2.501, 2.561, 4.205),(1.911, 2.561, 2.618)}	{(2.445, 2.501, 4.543),(1.921, 2.501, 2.558)}		
H14-N16	{**0**}	{(2.471, 2.530, 4.334),(1.916, 2.530, 2.592)}			
	{**-20**}{**+20**}	{(2.486, 2.545, 4.265),(1.913, 2.545, 2.606)}	{(2.457, 2.515, 4.419),(1.918, 2.515, 2.575)}		
	{**-40**}{**+40**}	{(1.898, 1.884, 1.902),(1.884, 1.884, 1.885)}	{(1.901, 1.887, 1.905),(1.886, 1.887, 1.887)}		
H17-N16	{**0**}	{(1.899, 1.885, 1.903),(1.885, 1.885, 1.885)}			
	{**-20**}{**+20**}	{(1.898, 1.885, 1.902),(1.884, 1.885, 1.885)}	{(1.901, 1.886, 1.904),(1.885, 1.886, 1.886)}		